OPEN

Three-dimensional Neuroretinal Rim Thickness and Visual Fields in Glaucoma: A Broken-stick Model

Wendy W. Liu, MD, PhD,† Michael McClurkin, MD, MPP,† Edem Tsikata, PhD,*† Pui-Chuen Hui, PhD,*† Tobias Elze, PhD,*† Ali R.C. Celebi, MD,*†‡ Ziad Khoueir, MD,*†§ Ramon Lee, MD,†‖ Eric Shieh, MD,†¶ Huseyin Simavli, MD,*†# Christian Que, MD,*†** Rong Guo, MS,* Johannes de Boer, PhD,†††‡‡§§ and Teresa C. Chen, MD*†*

Precis: In open-angle glaucoma, when neuroretinal rim tissue measured by volumetric optical coherence tomography (OCT) scans is below a third of the normal value, visual field (VF) damage becomes detectable.

Received for publication December 21, 2019; accepted June 6, 2020.

From the *Department of Ophthalmology, Massachusetts Eye and Ear; †Harvard Medical School; ††Massachusetts General Hospital, Wellman Center for Photomedicine, Boston, MA; §Beirut Eye and ENT Specialist Hospital, Saint-Joseph University Medical School, Beirut, Lebanon; ‖University of Southern California Roski Eye Institute; ¶Department of Ophthalmology, University of California, Los Angeles, CA; ‡Acibadem University School of Medicine, Istanbul; #Department of Ophthalmology, Pamukkale Universitesi, Denizli, Turkey; **Romblon Provincial Hospital, Romblon, Philippines; ‡‡LaserLaB Amsterdam, Department of Physics and Astronomy, Vrije Universiteit; and §§Department of Ophthalmology, VU Medical Center, Amsterdam, The Netherlands.

This work was conducted with support from Harvard Catalyst, The Harvard Clinical and Translational Science Center (National Center for Advancing Translational Sciences, National Institutes of Health Award UL 1TR002541) and financial contributions from Harvard University and its affiliated academic healthcare centers. The content is solely the responsibility of the authors and does not necessarily represent the official views of Harvard Catalyst, Harvard University and its affiliated academic healthcare centers, or the National Institutes of Health.

Disclosure: T.C.C.: Massachusetts Lions Eye Research Fund; American Glaucoma Society Mid-Career Award; National Institutes of Health UL1 RR 025758; Fidelity Charitable Fund; Department of Defense Small Business Innovation Research DHP 15-01615-016. J.F.B.: Center for Biomedical Optical Tomography Research and Translation Scientific Advisory Board Chair (Harvard Medical School); Licenses to NIDEK Inc., Terumo Corporation, Ninepoint Medical, and Heidelberg Engineering. T.E.: Massachusetts Lions Eye Research Fund; BrightFocus Foundation; Grimshaw-Gudewicz Foundation; Research to Prevent Blindness; Alice Adler Fellowship; National Institutes of Health R21EY030142, R21EY030631, R01EY030575, NEI Core Grant P30EY003790. US Provisional Applications No. 62/637,181; 62/641,785; 62/804,903; US Patent PCT/US2014/052414. The remaining authors declare no conflict of interest.

Reprints: Teresa C. Chen, MD, Massachusetts Eye and Ear, Glaucoma Service, 243 Charles Street, Boston, MA 02114 (e-mail: teresa_chen@meei.harvard.edu).

Supplemental Digital Content is available for this article. Direct URL citations appear in the printed text and are provided in the HTML and PDF versions of this article on the journal's website, www.glaucomajournal.com.

DOI: 10.1097/IJG.0000000000001604

Purpose: To determine the amount of neuroretinal rim tissue thickness below which VF damage becomes detectable.

Methods: In a retrospective cross-sectional study, 1 eye per subject (of 57 healthy and 100 open-angle glaucoma patients) at an academic institution had eye examinations, VF testing, spectral-domain OCT retinal nerve fiber layer (RNFL) thickness measurements, and optic nerve volumetric scans. Using custom algorithms, the minimum distance band (MDB) neuroretinal rim thickness was calculated from optic nerve scans. "Broken-stick" regression was performed for estimating both the MDB and RNFL thickness tipping-point thresholds, below which were associated with initial VF defects in the decibel scale. The slopes for the structure-function relationship above and below the thresholds were computed. Smoothing curves of the MDB and RNFL thickness covariates were evaluated to examine the consistency of the independently identified tipping-point pairs.

Results: Plots of VF total deviation against MDB thickness revealed plateaus of VF total deviation unrelated to MDB thickness. Below the thresholds, VF total deviation decreased with MDB thickness, with the associated slopes significantly greater than those above the thresholds ($P < 0.014$). Below 31% of global MDB thickness, and 36.8% and 43.6% of superior and inferior MDB thickness, VF damage becomes detectable. The MDB and RNFL tipping points were in good accordance with the correlation of the MDB and RNFL thickness covariates.

Conclusions: When neuroretinal rim tissue, characterized by MDB thickness in OCT, is below a third of the normal value, VF damage in the decibel scale becomes detectable.

Key Words: minimum distance band, optic nerve, spectral-domain optical coherence tomography

(*J Glaucoma* 2020;29:952–963)

The diagnosis of open-angle glaucoma (OAG) is usually made when there is already a functional visual field (VF) loss.[1,2] However, classic histology studies have suggested that by the time irreversible vision loss is detected on traditional white-on-white perimetry, about 40% of the optic nerve tissue is already irreversibly lost.[3] As a result, glaucoma can progress insidiously with substantial irreversible structural damage occurring before clinical intervention. Glaucoma is the second leading cause of blindness globally and affects over 2 million people in the United States,[4–6] with an overall prevalence of ~1.2% to 3%, with perhaps 11.3% of African Americans 80 years and older having the disease.[4,7,8] Early detection of glaucoma through structural monitoring of the optic nerve is critical for the timely management of this disease.

Optical coherence tomography (OCT) is an objective tool that can quantify glaucomatous structural damage and that simulates in vivo histology. Specifically, spectral-domain optical coherence tomography (SD-OCT) enables high-resolution, 3-dimensional (3D) imaging of optic nerve head (ONH) structure. The most commonly used parameter for detecting structural loss in glaucoma is the 2D peripapillary retinal nerve fiber layer (RNFL) thickness measurement.[9] However, there are limitations of the 2D-scan protocol, including a high frequency of imaging artifacts, high false-positive rates in myopic eyes, and intersubject variability in the ONH anatomy and dimensions.[10–13] These limitations prompted the development of more robust and stable diagnostic parameters from 3D volumetric OCT scans. Recently, it has been shown that harnessing the additional structural information from 3D OCT data provides at least the same, or better, diagnostic capabilities as RNFL thickness measurements in 2D, but with fewer artifacts.[14–21] In particular, two candidate 3D neuroretinal rim parameters, namely (1) the Bruch's membrane opening-minimum rim width (BMO-MRW) and (2) the minimum distance band (MDB) thickness, have been identified to better delineate the ONH geometry through OCT-derived features.[14,17,20,22] The BMO-MRW is defined by the minimum distance between the BMO and the inner limiting membrane (cup) surface and is calculated using a relatively low-density radial scan protocol.[23,24] It denotes the space through which the retinal nerve fibers are directed from the retina to the lamina cribosa. The MDB is a similar parameter, but uses the more easily identifiable BMO/retinal pigment epithelium (RPE) complex instead of BMO alone to define the disc border, and is calculated using a higher-density raster scan protocol.[17,23] The RPE/Bruch's membrane (BM) complex is likely a more robust OCT-based disc margin that is more consistently visible in SD-OCT images because the average BMO thickness is less than the axial resolution of commercially available SD-OCT machines.[17] The axonal loss at the ONH can be detected by quantifying any reduction in BMO-MRW or MDB thickness. The diagnostic capability of 3D neuroretinal rim parameters MDB and BMO-MRW has been compared with that of RNFL thickness. Most of the studies suggest that the diagnostic capabilities of MDB thickness and BMO-MRW were slightly better than RNFL thickness.[14,17,20,24] Specifically, in one study, it was reported that the area under the receiver-operator curve for diagnosing early glaucoma with the global MDB parameter was 0.952 with a sensitivity of 96.8% and specificity of 84.5%. Whereas for global RNFL thickness, the area under the receiver-operator curve was 0.928 with a sensitivity of 90.3% and specificity of 81.0%.[17] These results suggest that further investigation of the utility of 3D neuroretinal rim parameters is a worthwhile avenue for improving glaucoma diagnosis.

Previous studies have proposed models to correlate structural damage and functional vision loss in glaucoma.[25–27] One such model is the broken-stick tipping-point model, which identifies a threshold for structural loss at which VF damage becomes detectable and shows a significant correlation with structural parameters. The determination of this threshold value is of clinical importance, as it can aid in the diagnosis of glaucoma, and in counseling patients who have known glaucoma. This model was first used to obtain the threshold values for RNFL thicknesses in various sectors at which vision loss was first detected[2,27]; a similar analysis was also extended to the 3D BMO-MRW parameter and the threshold values were compared with the 2D counterparts.[28] Those studies reported a range of 8.4% to 17.3% of overall RNFL thickness decrease and 25.9% of overall BMO-MRW decrease when VF damage becomes detectable. In this study, we evaluate the structure-function correlation between MDB neuroretinal thickness and Humphrey visual field (HVF) testing in order to determine the amount of ONH tissue below which VF damage becomes detectable. In particular, we determine the MDB tipping point, or MDB neuroretinal rim value, below which significant VF damage occurs. Moreover, we assess the correspondence of the independently extracted MDB neuroretinal rim tipping points and the RNFL thickness tipping points.

METHODS

Data Collection

We did a retrospective review of patients who were seen in the Glaucoma Service at the Massachusetts Eye and Ear between September 2009 and July 2014, and who were a cross-sectional sampling of the larger prospective SD-OCT in Glaucoma study. Study protocols were approved by the Massachusetts Eye and Ear Institutional Review Board and were in accordance with the Health Insurance Portability and Accountability Act. The research adhered to the tenets of the Declaration of Helsinki for research involving human subjects.

Subjects were included if they were either healthy volunteers or OAG patients of age 18 years or older. Subjects were excluded if any of the following was present: corneal scarring, media opacities, anterior segment dysgenesis, past chronic steroid use, history of diabetic retinopathy, or any other disease or medical treatment that might independently affect VF or retinal thickness. Other exclusion criteria included a history of intraocular surgery except for uncomplicated cataract extraction at least a year before enrollment, and best-corrected visual acuity worse than 20/40. In addition, patients with refractive error outside the −6.00 to +6.00 diopter range were excluded as the optic discs of highly myopic eyes are shown to seem anomalous, which impacts the OCT image quality and reliability.[29,30]

Normal subjects were those without the ocular disease, except for mild cataracts, and those with normal HVF test results. The cup to disc ratio was 0.4 or less for Whites and 0.6 or less for Asians, African Americans, and Hispanics. Glaucoma patients were defined as having characteristic changes of the ONH with corresponding abnormal VF defects. An abnormal HVF was defined by either 3 or more contiguous pattern standard deviation (PSD) test locations depressed by 5 dB or more; or 2 or more contiguous PSD test locations with 1 depressed by 10 dB or more and the other by 5 dB or more. Abnormal PSD test locations on the outer rim of the VF were not considered in the aforementioned criteria to account for peripheral rim artifacts. Both primary OAG and normal-tension glaucoma, as well as secondary OAG (pigmentary glaucoma and pseudoexfoliation glaucoma) patients were included. All diagnoses were confirmed by a glaucoma specialist (T.C.C.). One eye of each subject was randomly selected for analysis.

Eye Examination

All patients had a complete history and eye examination by a glaucoma specialist (T.C.C.). Clinical data obtained included best-corrected visual acuity, Goldman

applanation tonometry, slit-lamp biomicroscopy, gonioscopy, pachymetry (PachPen; Accutome Ultrasound Inc., Malvern, PA), and dilated fundus examination. Age, race, sex, and spherical equivalent refractive error were recorded for all patients.

VF Testing

Swedish Interactive Threshold Algorithm (SITA) 24-2 testing by the HVF analyzer 750i (Carl Zeiss Meditec, Dublin, CA) was performed on all subjects. Reliable VF tests had false-positive and false-negative rates of $\leq 20\%$ and fixation losses of $\leq 33\%$.

VF total deviation (TD) values were recorded for all 52 testing points. The individual HVF values were grouped to correspond to regions of the ONH. This structure-function correlation was modeled after the Garway-Heath map.[31] TD values were unlogged, and the average of all unlogged values in each group was log-transformed back to decibel scale.[26]

SD-OCT Imaging

All patients had 3D SD-OCT scans of the ONH (Spectralis; Heidelberg Engineering, Heidelberg, Germany). The Spectralis OCT has a scan speed of 40,000 A-lines per second with real-time eye movement tracking.[32,33] From 3D optic nerve 193-line raster volume scans, the MDB neuroretinal rim thickness was calculated using custom-designed software.[14–16] The MDB borders were automatically detected, with the outer border ring as the RPE/BM termination or OCT-based disc boundary and the inner border ring at the ONH surface. The MDB neuroretinal rim thickness values were calculated for global values and quadrant values. Images of scan quality below 15 were excluded.

Statistical Methods

A scatter plot was used to show the relationship between MDB neuroretinal rim parameters and VF values (in dB) and between RNFL thickness and VF values (in dB). Statistical analyses were performed with MATLAB (The Mathworks Inc., Natick, MA) and SAS 9.4 (SAS Institute Inc., Cary, NC). A series of broken-stick regression models were then fitted into the data using a nonlinear fitting routine where the fitting parameters are the tipping point, the slopes below and above the tipping point, and the intercept. The model with the least root mean-squared error was chosen as the final model. The tipping point from the final model was reported, along with the slopes below the tipping point and their corresponding 95% confidence intervals (CIs). Using the mean MDB and RNFL thickness values for the normal subjects in our cohort, the percentage of MDB and RNFL loss necessary to reach the tipping point was also calculated for the mean global, quadrant, and sector MDB and RNFL thickness values. We also performed a lowess smoothing fit to delineate a nonparametric relationship between the VF values and the structural parameters, with which the broken-stick fit was compared.

We then checked whether the independently obtained tipping points for MDB thickness were consistent with those for RNFL thickness. Specifically, we first used a scatter plot to illustrate the relationship between the RNFL thickness and the MDB thickness. We performed a lowess smoothing fit to delineate a nonparametric relationship between these 2 covariates. The corresponding confidence bounds for the lowess fit at the 95% CI were obtained by 5000 iterations of bootstrapping. Subsequently, for each region, a point whose coordinates are given by (MDB tipping point, RNFL tipping point), was plotted on the scatter plot. The 95% CIs of the tipping points corresponding to both the MDB and RNFL thicknesses were also shown. The Spearman correlations between the RNFL thickness and the MDB thickness were calculated with the corresponding *P*-values. Results were expressed as means ($\pm$SD) unless otherwise stated. *P*-values of <0.05 established statistical significance.

RESULTS

Table 1 summarizes the demographics of the 157 study subjects (57 healthy and 100 OAG patients). Of all 157 subjects, 55% were female and 65% were White. Of the OAG patients, 67 had primary OAG, 14 had pseudoexfoliation glaucoma, 8 had pigmentary glaucoma, and 11 had normal-tension glaucoma. Table 1 shows that healthy and glaucoma subjects were statistically different, in that the glaucoma group was older (ie, 67.9 vs. 54.2 y; $P < 0.0001$), had worse HVFs (ie, MD, −12.2 vs. −1.5 dB; PSD, 8.5 vs. 1.5 dB; $P < 0.0001$), and had thinner MDB neuroretinal rim thickness values (174.3 vs. 312.8 μm).

Figure 1 depicts the structure-function relationship between global MDB neuroretinal rim thickness and global VF TD (in dB). For healthy eyes with normal VFs (Fig. 1, red squares), the structure-function relationship displayed a plateau, with neuroretinal rim thickness values being unrelated to VF values. Then a tipping point occurred at 216 μm (Fig. 1, yellow circle; Table 2), below which MDB neuoretinal thickness values exhibited a strong relationship with VF values. We compared the slopes below and above the tipping point (0.086 vs. 0.011 dB/μm), and they are significantly different ($P < 0.001$; Table 3). This shows that the existence of the tipping point, or the threshold phenomenon, is significant. Specifically, the tipping point for mean MDB neuroretinal thickness was 216 μm (Table 2; Fig. 1) and was 31.0% below the mean normal value (313 ± 41 μm; Table 2).

Next in Figure 2, we used the same methodology to investigate the structure-function correlation and tipping points for each quadrant by correlating the quadrant average MDB neuroretinal rim thickness (ie, superior, nasal, inferior, temporal) with the corresponding average VF TD (ie, inferior, temporal, superior, nasal). For the superior and inferior quadrants, which are typically the first sites of glaucomatous damage, the respective fitted tipping points are 218 and 197 μm with 95% CI widths of ± 30 and 33 μm (Table 2). Comparing them with their respective mean

TABLE 1. Demographics and Clinical Characteristics of the 157 Healthy and Glaucomatous Subjects Who Had 3-dimensional Optic Nerve Head Spectral-domain OCT Imaging

Characteristics	Healthy (n = 57)	Glaucoma (n = 100)	*P*
Age (y)	54.2 ± 15.5	67.9 ± 11.9	<0.0001*
Female/male (%)	39/18 (68.4)	47/53 (47.0)	0.01*
Visual field MD (dB)	−1.5 ± 1.9	−12.2 ± 7.5	<0.0001*
Visual field PSD (dB)	1.5 ± 0.3	8.5 ± 3.1	<0.0001*
OCT MDB neuroretinal rim (μm)	312.8 ± 41.4	174.3 ± 51.1	<0.0001*

Results are expressed as means ± SD.

MD indicates mean deviation; MDB, minimum distance band; OCT, optical coherence tomography; PSD, pattern standard deviation.

*Statistically significant ($P < 0.05$).

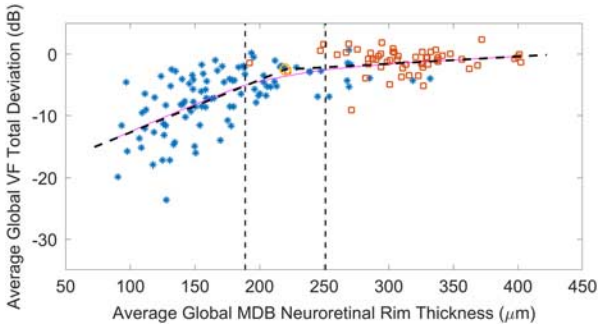

FIGURE 1. Neuroretinal rim broken-stick model for global values: determining the tipping point at which global neuroretinal rim thinning is first associated with visual field (VF) damage. This graph correlates minimum distance band (MDB) neuroretinal rim values (*x*-axis) with corresponding VF total deviation values (*y*-axis) for 157 healthy and glaucomatous eyes, where each of the 52 total deviation points were unlogged, averaged, then log-transformed back to decibel scale. Broken-stick model is represented by the dashed diagonal black line with the lowess smoothing fit in pink. Red squares represent healthy eyes. Blue stars represent glaucoma eyes. The yellow open circle represents the tipping point of global MDB thickness, with the 95% confidence interval indicated by vertical dashed lines.

normal MDB thickness values (345 ± 59 μm and 349 ± 49 μm; Table 2), the tipping point occurred after a 36.8% and 43.6% damage in the superior and inferior quadrants (Table 2). The fitted tipping points in the nasal and temporal quadrants are 220 and 167 μm with 95% CI widths of ± 50 and ± 29 μm, respectively (Table 2). Comparing them with their respective mean normal MDB thickness values (312 ± 49 um and 246 ± 42 μm; Table 2), the tipping point occurred after a 29.6% and 32.1% damage in the nasal and temporal quadrants, respectively (Table 2). The corresponding VF TD values at these tipping points ranged between −2.9 and −4.4 dB. To verify the non-negligible existence of the tipping points in each quadrant, Table 3 shows that the slopes for VF TD as a function of MDB thickness below the tipping points were significantly steeper than the slopes above the threshold in all 4 quadrants (*P*-value <0.05; last column of Table 3). The slopes, which indicate the rate of VF loss as a result of the MDB thickness reduction below the tipping points, are given by 0.108 dB/μm (superior quadrant), 0.143 dB/μm (inferior quadrant), 0.070 dB/μm (nasal quadrant), and 0.091 dB/μm (temporal quadrant).

In Figure 3, we also assessed the structure-function correlation in each 45-degree sector [ie, superior-nasal (SN), superior-temporal (ST), inferior-nasal (IN), and inferior-temporal (IT)] by correlating the sector average MDB thickness with the average VF TD of the corresponding sector. As tabulated in Table 3, the fitted tipping points are located at 238 μm (SN; 95% CI width = 43 μm), 211 μm (ST; 95% CI width = 36 μm), 233 μm (IN; 95% CI width = 44 μm), and 210 μm (IT; 95% CI width = 62 μm), respectively. Referencing to their normal MDB thickness, that is, 352 ± 63 μm (SN), 346 ± 57 μm (ST), 360 ± 56 μm (IN), and 339 ± 51 μm (IT), the tipping points occurred after an MDB thickness reduction of 32.3% (SN), 39.1% (ST), 35.1% (IN), and 38.2% (IT). The corresponding VF TD values at these tipping points ranged between −3.3 and −4.1 dB. The slopes below the tipping points, 0.09 dB/μm (SN), 0.116 dB/μm (ST), 0.111 dB/μm (IN), and 0.103 dB/μm (IT), are all significantly different from the slopes above their respective tipping points in all 4 sectors (last column of Table 3).

In Figures 4–6, we performed the broken-stick regression analysis for RNFL thickness with the corresponding global, quadrant, and sectorial data, in order to compare this with MDB neuroretinal rim thickness data (Table 4). For global RNFL thickness, the tipping point is at 70 μm (Table 4), below which VF damage occurs. This 70 μm tipping point value represents a 26.6% overall RNFL decrease from normative RNFL values (ie, 95 μm; Table 4), versus the MDB neuroretinal rim tipping point of 216 μm or a 31.0% overall MDB neuroretinal rim decrease (Tables 2, 4) compared with normative MDB values (ie, 313 μm; Table 2). For the superior and inferior RNFL quadrants, respective tipping points are at 82 and 72 μm, or 28.2% and 41.7% relative to the mean normal thickness (Table 4). The slopes below and above the RNFL tipping points are all statistically different for the global, quadrant, and sectorial data (*P*-values from <0.001 to 0.008), except for the nasal quadrant (*P* = 0.066; Table 5).

With Table 6 and Figure 7, we evaluated the correlation between the MDB thickness and the RNFL thickness and whether the independently obtained tipping points for MDB thickness are consistent with those for RNFL thickness. With the Spearman correlation coefficients ~0.638 to 0.889 across all regions (Table 6), the MDB thickness shows a strong positive monotonic correlation with the RNFL thickness. Figure 7 shows the scatter plots of RNFL

TABLE 2. The Neuroretinal Rim MDB Tipping Point Values, Which are Associated With Initial Visual Field Damage, are Shown as Absolute Values and as Percentage Tissue Decrease, as Measured by Spectral-domain Optical Coherence Tomography Volume Scans

Anatomic Region	MDB Tipping Point [95% CI] (μm)	Mean MDB Thickness of Normal (μm)	MDB Tipping Point Relative to Mean MDB Thickness of Normal (%)
Global	216.0 [185.6, 246.3]	312.8 ± 41.4	31.0
Superior	218.1 [188.3, 248.0]	345.2 ± 59.1	36.8
Inferior	197.2 [163.6, 230.7]	349.5 ± 48.8	43.6
Nasal	219.7 [169.9, 269.4]	312.0 ± 49.4	29.6
Temporal	166.7 [137.6, 195.8]	245.6 ± 42.0	32.1
Superior-nasal	238.0 [195.4, 280.6]	351.6 ± 62.8	32.3
Superior-temporal	210.7 [175.1, 246.3]	346.3 ± 56.9	39.1
Inferior-nasal	233.4 [188.7, 278.1]	359.7 ± 56.5	35.1
Inferior-temporal	209.6 [148.0, 271.2]	339.3 ± 51.0	38.2

Results are expressed as means ± SD, unless otherwise stated.
CI indicates confidence interval; MDB, minimum distance band.

TABLE 3. The Neuroretinal Rim Broken-stick Model With Associated Slopes Above and Below the Tipping Point, the Point at Which MDB Neuroretinal Rim Thinning is First Associated With Visual Field Damage

Anatomic Region	Slope Below the Tipping Point [95% CI] (dB/µm)	P*	Slope Above the Tipping Point [95% CI] (dB/µm)	P†	Difference Between Slopes Below and Above the Tipping Points (dB/µm)	P‡
Global	0.086 [0.063, 0.108]	<0.001	0.011 [−0.025, 0.048]	0.266	0.074	<0.001
Superior	0.108 [0.080, 0.136]	<0.001	0.010 [−0.033, 0.053]	0.319	0.097	<0.001
Inferior	0.143 [0.101, 0.185]	<0.001	0.018 [−0.045, 0.081]	0.286	0.125	<0.001
Nasal	0.070 [0.044, 0.097]	<0.001	0.013 [−0.031, 0.056]	0.280	0.058	0.014
Temporal	0.091 [0.058, 0.124]	<0.001	0.017 [−0.033, 0.066]	0.256	0.074	0.007
Superior-nasal	0.090 [0.061, 0.120]	<0.001	0.011 [−0.036, 0.057]	0.327	0.080	0.003
Superior-temporal	0.116 [0.080, 0.152]	<0.001	0.011 [−0.042, 0.065]	0.339	0.105	0.001
Inferior-nasal	0.111 [0.073, 0.148]	<0.001	0.019 [−0.039, 0.077]	0.260	0.092	0.005
Inferior-temporal	0.103 [0.063, 0.142]	<0.001	0.016 [−0.047, 0.080]	0.304	0.086	0.012

All *P*-values are taken as statistically significant when $P < 0.05$.
**P*-values for the slopes below the tipping points represent the statistical significance of the slopes being different than 0.
†*P*-values for the slopes above the tipping points represent the statistical significance of the slopes being different than 0.
‡*P*-values for the last column represent the statistical significance of the difference between the slopes below the tipping points and above the topping point.
CI indicates confidence interval; MDB, minimum distance band.

thickness against MDB thickness for the global average, the 4 quadrants, and the 4 sectors. There, a region, bounded by the 95% CIs of both the tipping points, encompassed the upper and lower confidence bounds of the lowess fit for all the quadrants and sectors. This suggests that the correspondence and consistency of the RNFL tipping points with their MDB counterparts respect the nonparametric correlation relationship of the RNFL and MDB thicknesses.

DISCUSSION

In this cross-sectional study, we use the broken-stick model to identify an MDB neuroretinal rim tipping point, below which VF loss generally becomes detectable in the decibel scale. (For completeness, we also performed the broken-stick analysis on the unlogged VF TD data, which is presented in Supplemental Information section I, Fig. S1 and Table S1, Supplemental Digital Content 1, http://links.lww.com/IJG/A453.) This study shows that below 31.0% of global MDB neuroretinal rim thickness, VF damage becomes detectable, which corresponds to MDB thickness of 216 µm (Table 2; Fig. 1). Neuroretinal rim parameters such as the MDB thickness are of clinical interest because they are designed to provide objective quantification of the nerve tissue in the neuroretinal rim.[23] Our results are consistent with previous structure-function studies in glaucoma, which found that substantial nerve tissue loss, namely 8.4% to 17.3% in RNFL and 25.9% in BMO-MRW, occurs before clinically detectable VF damage.[2,26–28,34–38] This is possibly because in the early stages of glaucoma, current VF tests do not have high sensitivity to early loss compared with structural measurements.[26,38] Hence, tests of structure may be better suited for detecting early disease in glaucoma, whereas VF-based tests of function may be better for

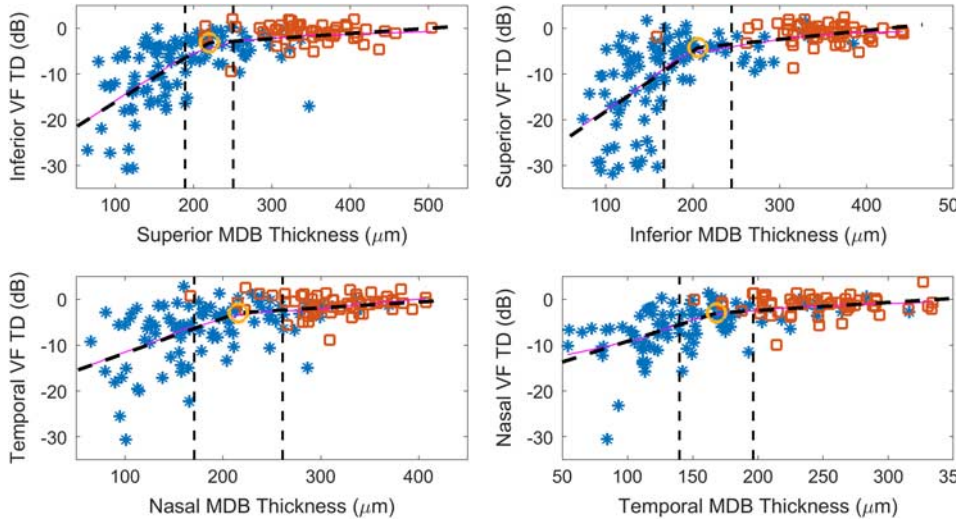

FIGURE 2. Neuroretinal rim broken-stick model for quadrant values: determining the tipping point at which quadrant neuroretinal rim thinning is first associated with visual field (VF) damage. This graph correlates minimum distance band (MDB) neuroretinal rim values (*x*-axis) with corresponding VF total deviation (TD) values (*y*-axis) for 157 healthy and glaucomatous eyes for each of the 4 quadrants. Broken-stick models are represented by the dashed diagonal black lines with the lowess smoothing fit in pink. Red squares represent healthy eyes. Blue stars represent glaucoma eyes. The yellow open circles represent the tipping points, with the 95% confidence interval indicated by vertical dashed lines.

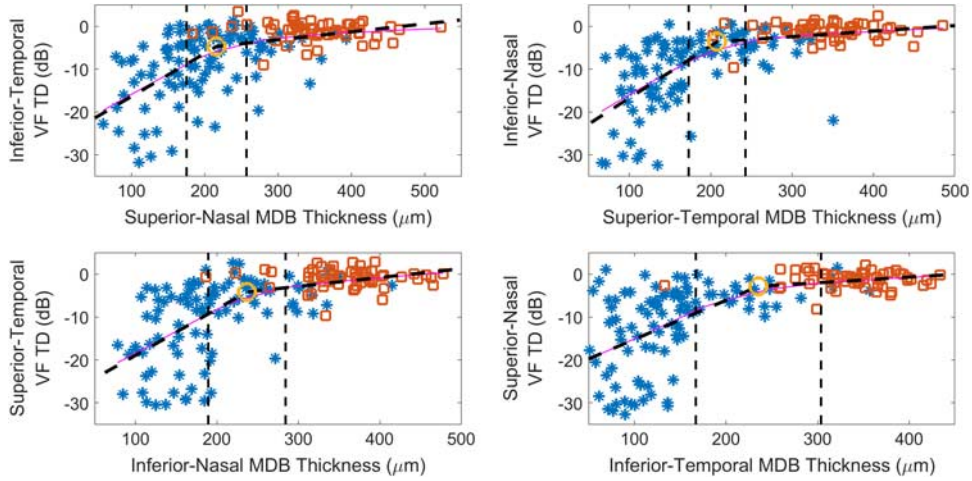

FIGURE 3. Neuroretinal rim broken-stick model for sector values: determining the tipping point at which sector neuroretinal rim thinning is first associated with visual field (VF) damage. This graph correlates minimum distance band (MDB) neuroretinal rim values (*x*-axis) with corresponding VF total deviation (TD) values (*y*-axis) for healthy and glaucomatous eyes for each of the 4 sectors. Graphs are presented for average VF TD for each of the 4 sector values versus the corresponding MDB values. Broken-stick model is represented by the dashed black line with the lowess smoothing fit in pink. Red squares represent healthy eyes. Blue stars represent glaucoma eyes. The yellow open circles represent the tipping points, with the 95% confidence interval indicated by vertical dashed lines.

detecting late disease, as suggested by prior histology and disc photography assessment.[2,27,39,40] In the future, however, other imaging modalities and electro/optophysiological functional tests may confer higher sensitivities for probing dysfunctional retinal ganglion cells, enabling early detection of glaucoma and establishing the structure-function relationship even in the early stage.[41]

Nine of 100 of the glaucomatous subjects (9%) fall outside of the upper CI of the tipping point and within the global MDB-VF TD range of the normal subjects. Hence, it is important to inspect the quadrant and the sectorial data as well because focal VF damage may not be evident in the global characterization. The observations that significant neuroretinal tissue loss is present when VF damage becomes detectable also hold true for the quadrant and sectorial data. In particular, the percentage loss of structure when VF damage is detected in all 4 quadrants range from 29.6% to 43.6% (Table 2). For the sectorial data, the sectors share a similar percentage loss of structure when VF damage is detected, ranging from 32.3% to 39.1% (Table 2). Furthermore, monitoring the structural variations in these quadrants/ sectors is crucial as loss of neuroretinal tissues in these regions cannot be sensitively detected by functional assessment alone. The percentage loss of MDB thickness was calculated referencing to the average MDB thickness from the normal subjects, which forms a modest cohort size (n = 57). In the future, it would be interesting to study age-matched values of MDB thicknesses from a larger cohort of nonglaucomatous subjects and adjust for age-related MDB thickness reduction.

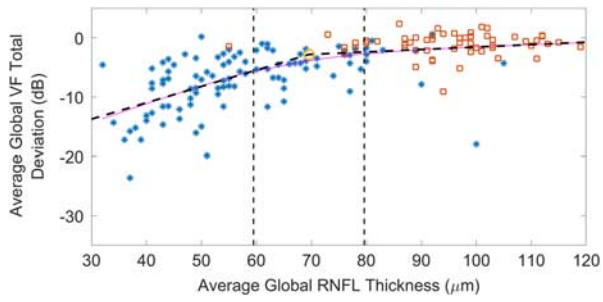

FIGURE 4. Retinal nerve fiber layer (RNFL) broken-stick model for global values: determining the tipping point at which global RNFL thinning is first associated with visual field (VF) damage. This graph correlates RNFL values (*x*-axis) with corresponding VF total deviation values (*y*-axis) for healthy and glaucomatous eyes, where each of the 52 testing points were unlogged, averaged, then log-transformed back to decibel scale. Graphs are presented for average VF total deviation values versus the global RNFL values. Broken-stick model is represented by the dashed black line with the lowess smoothing fit in pink. Red squares represent healthy eyes. Blue stars represent glaucoma eyes. The yellow open circle represents the tipping point, with the 95% confidence interval indicated by vertical dashed lines.

In the broken-stick model, which does not guarantee the presence of a tipping point, the necessary condition for the existence of a tipping point is that the fitted slopes below and above the tipping point are significantly different. On the contrary, when the fitted slopes of the 2 segments are not significantly different, the fitted broken-stick model is essentially similar to a linear model and a tipping point does not exist in this case. In our study, the slopes below the tipping points in all quadrants were significantly steeper than those above the tipping points, characterized by a *P*-value <0.02 (Table 3). Furthermore, the slopes above the tipping points were all not significantly different from 0. Together these findings suggest that a thresholding phenomenon for MDB reduction does exist for all quadrants and sectors. In addition, the slopes above the tipping points are not significantly different from 0, echoing previous findings that initial neuroretinal tissue loss, defined by the MDB thickness in this study, does not lead to significant VF damage until the tipping-point threshold is reached. Furthermore, the magnitude of the fitted slopes may also inform clinicians about the degree of VF decline as a result of further structural loss and provide information regarding which quadrants and sectors of neuroretinal tissues are more

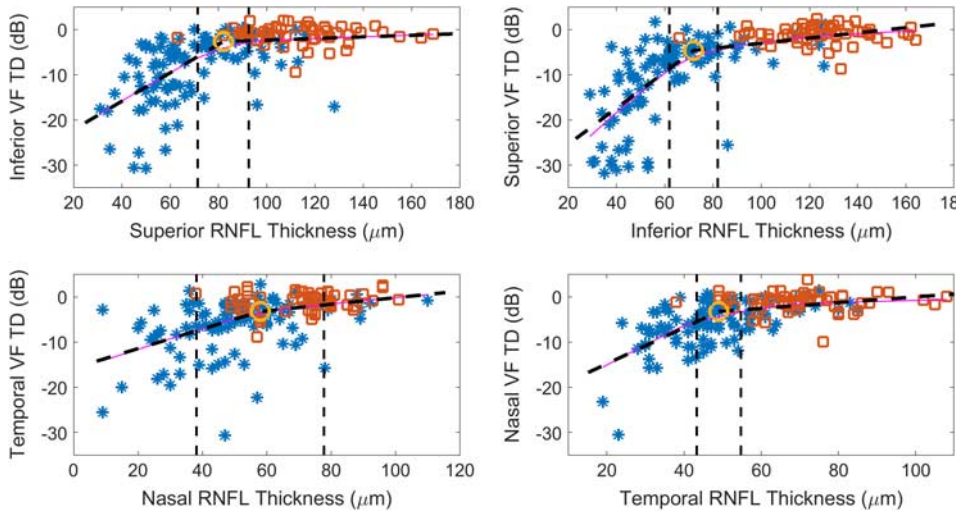

FIGURE 5. Retinal nerve fiber layer (RNFL) broken-stick model for quadrant values: determining the tipping point at which quadrant RNFL thinning is first associated with visual field (VF) damage. This graph correlates RNFL values (*x*-axis) with corresponding VF total deviation (TD) values (*y*-axis) for healthy and glaucomatous eyes, where each of the 52 testing points were unlogged, averaged, then log-transformed back to decibel scale. Graphs are presented for average VF TD values versus the quadrant RNFL values. Broken-stick model is represented by the dashed black line with the lowess smoothing fit in pink. Red squares represent healthy eyes. Blue stars represent glaucoma eyes. The yellow open circles represent the tipping points, with the 95% confidence interval indicated by vertical dashed lines.

vulnerable and in need of more frequent monitoring to prevent further neuroretinal tissue loss. The caveat of utilizing the VF damage rate as a function of their structural parameter below the tipping point is that several quadrants and sectors (eg, inferior, IN, ST, IT) consist of rather large VF TD variability (spanning 20 to 30 dB) for certain thicknesses below the tipping point. One may speculate that a simple linear fit may not satisfactorily characterize the structure-function relationship. To address this, we performed a lowess fit to the structure-function data, and verified that the current broken-stick model overlapped excellently with the lowess fit, except expectedly for the regions around the tipping points. Further studies, including the consideration of the floor effects and the extent of individual variability, are needed to explain the wide variability in the VF TD and examine its influence on the description of the structure-function correlation.

Our study also directly compared the structure-function relationship on the basis of both the neuroretinal rim parameter, namely the MDB thickness and the previously explored RNFL thickness. Notably, the tipping point for the nasal quadrant was not statistically significant for the RNFL data, but was identified to be significant in the MDB data. The difficulty in identifying a statistically significant tipping point for the nasal quadrant using the RNFL data were previously reported by Wollstein et al.[27] Our study

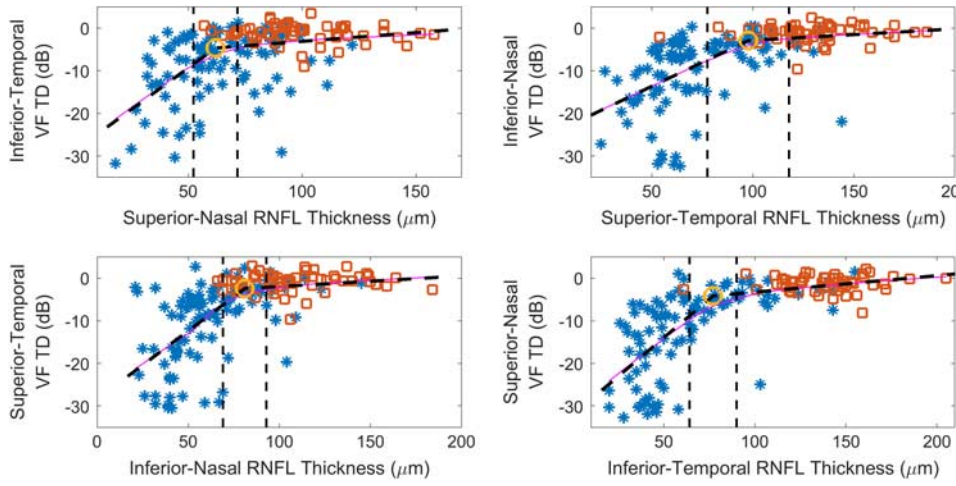

FIGURE 6. Retinal nerve fiber layer (RNFL) broken-stick model for sector values: determining the tipping point at which sector RNFL thinning is first associated with visual field (VF) damage. This graph correlates RNFL values (*x*-axis) with corresponding VF total deviation (TD) values (*y*-axis) for healthy and glaucomatous eyes, where each of the 52 testing points were unlogged, averaged, then log-transformed back to decibel scale. Graphs are presented for average VF TD values versus the sectoral RNFL values. Broken-stick model is represented by the dashed black line with the lowess smoothing fit in pink. Red squares represent healthy eyes. Blue stars represent glaucoma eyes. The yellow open circles represent the tipping point, with the 95% confidence interval indicated by vertical dashed lines.

TABLE 4. The RNFL Tipping Point Values, Which are Associated With Initial Visual Field Damage, Are Shown as Absolute Values and as Percentage Tissue Decrease, as Measured by Spectral-domain Optical Coherence Tomography

Anatomic Region	RNFL Tipping Point [95% CI] (μm)	Mean RNFL Thickness of Normal (μm)	RNFL Tipping Point Relative to Mean RNFL Thickness of Normal (%)	MDB Tipping Point Relative to Mean MDB Thickness of Normal (%)
Global	69.6 [59.5, 79.6]	94.8 ± 12.1	26.6	31.0
Superior	82.0 [71.4, 92.6]	114.3 ± 20.3	28.2	36.8
Inferior	72.0 [62.0, 82.0]	123.4 ± 19.6	41.7	43.6
Nasal	58.0 [38.2, 77.8]	71.0 ± 14.0	18.3*	29.6
Temporal	49.0 [42.8, 55.2]	70.0 ± 14.0	30.0	32.1
Superior-nasal	62.0 [52.4, 71.6]	99.4 ± 22.9	37.6	32.3
Superior-temporal	97.8 [77.6, 118.0]	129.4 ± 23.5	24.4	39.1
Inferior-nasal	81.0 [69.0, 93.0]	108.3 ± 27.1	25.2	35.1
Inferior-temporal	77.1 [64.1, 90.0]	138.8 ± 23.3	44.5	38.2

Results are expressed as means ± SD, unless otherwise stated.
*Tipping point not significant.
CI indicates confidence interval; MDB, minimum distance band; RNFL, retinal nerve fiber layer.

attained a similar result but shows that the MDB thickness could instead serve as a substitute in uncovering the threshold phenomenon for all regions. Another interesting finding from this direct comparison is that the tipping points independently identified for the MDB data and for the RNFL data are in accordance with the correlation of the RNFL thickness and the MDB thickness. Given the same physiological origin of the neuroretinal rim and the RNFL, we anticipate that the locations of the tipping points for the MDB data should match with those for the RNFL data. Indeed, the one-to-one correspondence in this study is remarkable for the global average, and for all of the quadrants and sectors. The self-consistency demonstrated in these 2 independent broken-stick analyses lent further assurance in the locations of the fitted tipping points.

We compare our results with a previous study by Park and colleagues that used the broken-stick model to identify the tipping point at which the BMO-MRW, a similar neuroretinal rim parameter, began to show significant association with VF abnormalities. They found that 25.9% decrease of BMO-MRW thickness is necessary before VF damage occurs.[28] This is in good agreement with our study, which noted a 31.0% decrease (Table 4). As for the quadrant percentage decrease, they reported a 34.4% decrease in the nasal quadrant and 24.7% decrease in the temporal quadrant, comparing with a 23.2% decrease and 18.9% in our study. For the sectorial percentage decrease, they reported a 34.9% (SN), 8.9% (ST), 24.7% (IN), and 33.1% (IT) decrease, compared with a 32.3% (SN), 39.1% (ST), 35.1% (IN), and 38.2% (IT) decrease in our study. There are a few differences between our study and the study by Park and colleagues. First, the study by Park and colleagues included a similar number of subjects who were all of the Asian ethnicity, whereas 65% of subjects in our study population were White. Second, the BMO-MRW is a slightly different neuroretinal rim parameter than MDB, as it uses a radial scan protocol and the BM alone to define the OCT-based disc border, whereas the MDB uses a higher-density raster scan protocol and the RPE/BM complex as the border definition.[23] A previous study did not show any significant difference between the diagnostic capabilities of 3D neuroretinal rim parameters derived from raster scans such as MDB thickness versus those derived from radial scans such as BMO-MRW.[14] However, the raster scan may have some advantages in image acquisition time and the number of additional volumetric parameters produced, such as cup volume, peripapillary RNFL volume, and peripapillary retinal volume.[14,19] Whether a multivariate model exploiting

TABLE 5. The RNFL Broken-stick Model With Associated Slopes Above and Below the Tipping Point, the Point at Which RNFL Thinning is First Associated With Visual Field Damage

Anatomic Region	Slope Below the Tipping Point [95% CI] (dB/μm)	P*	Slope Above the Tipping Point [95% CI] (dB/μm)	P†	Difference Between Slopes Below and Above the Tipping Points (dB/μm)	P‡
Global	0.276 [0.192, 0.360]	< 0.001	0.04 [−0.095, 0.177]	0.275	0.235	0.002
Superior	0.314 [0.217, 0.412]	< 0.001	0.018 [−0.132, 0.168]	0.407	0.297	0.001
Inferior	0.400 [0.291, 0.509]	< 0.001	0.057 [−0.105, 0.219]	0.243	0.343	< 0.001
Nasal	0.216 [0.129, 0.302]	< 0.001	0.072 [−0.094, 0.239]	0.195	0.144	0.066
Temporal	0.399 [0.268, 0.531]	< 0.001	0.063 [−0.130, 0.256]	0.239	0.336	0.003
Superior-nasal	0.390 [0.245, 0.535]	< 0.001	0.041 [−0.173, 0.255]	0.352	0.349	0.004
Superior-temporal	0.225 [0.140, 0.310]	< 0.001	0.027 [−0.111, 0.165]	0.350	0.198	0.008
Inferior-nasal	0.321 [0.236, 0.406]	< 0.001	0.025 [−0.113, 0.162]	0.362	0.296	< 0.001
Inferior-temporal	0.362 [0.262, 0.462]	< 0.001	0.039 [−0.111, 0.188]	0.305	0.323	< 0.001

All *P*-values are taken as statistically significant when $P < 0.05$.
**P*-values for the slopes below the tipping points represent the statistical significance of the slopes being different than 0.
†*P*-values for the slopes above the tipping points represent the statistical significance of the slopes being different than 0.
‡*P*-values for the last column represent the statistical significance of the difference between the slopes below the tipping points and above the topping point.
CI indicates confidence interval; RNFL, retinal nerve fiber layer.

TABLE 6. Spearman Correlations Between the RNFL Thickness and the MDB Thickness

Anatomic Region	Spearman Correlations	*P*
Global	0.843	< 0.001
Superior	0.854	< 0.001
Inferior	0.864	< 0.001
Nasal	0.643	< 0.001
Temporal	0.723	< 0.001
Superior-nasal	0.768	< 0.001
Superior-temporal	0.826	< 0.001
Inferior-nasal	0.790	< 0.001
Inferior-temporal	0.858	< 0.001

MDB indicates minimum distance band; RNFL, retinal nerve fiber layer.

these additional volumetric parameters may afford further insights in monitoring glaucoma progression warrants future study.

Several previous studies have used the broken-stick model to study the relationship between RNFL thickness and VF damage.[2,27,42] Wollstein et al[27] found that 17.3% of RNFL thickness loss was needed before functional vision damage could be detected. Similarly, Alasil et al[2] found that ~8.4% of global RNFL thinning was necessary for damage to be detectable on VF testing. Moreover, in a recent study that investigated the impairment of retinal structures and visual cortex activity before VF damage in glaucoma, Murphy et al[42] reported a 14.4% of RNFL thickness loss before detectable VF damage. In comparison, we find in our study that at least 31.0% of global MDB thinning and 26.6% of global RNFL thinning are necessary to detect functional vision damage (Table 2; Fig. 1). The differences in the reported percentages in these studies can be because of (1) variability in the number of recruited glaucoma patients, (2) the percentage of those with mild versus severe glaucoma, and (3) differences in statistical methods used to fit the broken-stick model. In particular, the average VF MD of the glaucomatous cohort is −12.2 dB, which is rather advanced compared with other studies where the average VF MD of the glaucomatous cohort were in the range of −7 to −5 dB.[2,27,42] Heuristically, the data points in the glaucomatous cohort have weightier contributions by the advanced glaucoma subjects than by the early glaucoma/glaucoma suspect subjects. This may lead to a steeper slope in the linear fit among the glaucomatous group, which results in a tipping point that corresponds to lower MDB and RNFL thickness values. These findings together suggest that a lower percentage of RNFL thinning is required compared with the amount of neuroretinal rim thinning that occurs before clinically detectable VF damage. The higher percentage of neuroretinal rim width thinning required for VF damage may be because of an increased amount of nerve tissue in the ONH compared with the RNFL. A study of rhesus monkeys showed that the ONH, of which MDB is a cross-section, consists of ~94% ganglion cell nerve axons and 5% non-neural tissue.[43] Thus, nerve tissue is the main structure in the MDB. In contrast, 48.8% to 65.1% of the total RNFL thickness may be retinal glial cells (Müller cells, astroglia, microglia) and vessels that do not degenerate in the same manner as retinal ganglion cell axons, causing a "floor effect" in the RNFL thickness.[26,44–46] Hence, the

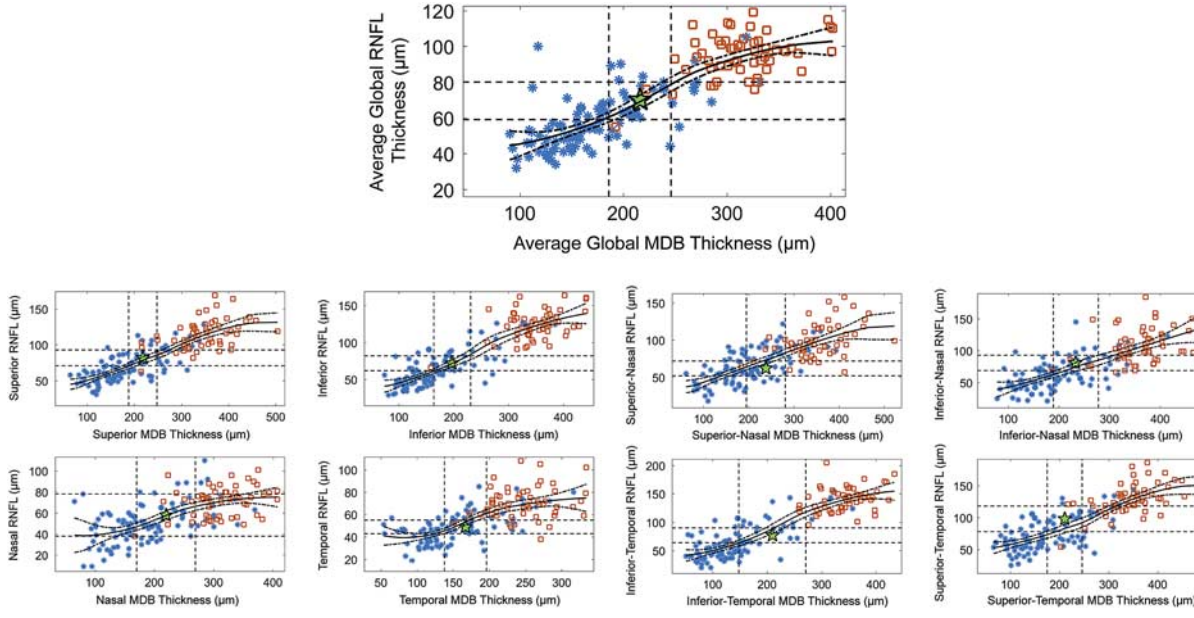

FIGURE 7. Correspondence of the independently determined tipping points for minimum distance band (MDB) neuroretinal rim thickness and retinal nerve fiber layer (RNFL) thickness for the global, quadrant, and sector values. The graph shows the correlation of the RNFL thickness (*y*-axis) with the MDB thickness (*x*-axis) for the global average, the 4 quadrants, and the 4 sectors. A point with coordinates given by the independently determined MDB tipping point and the RNFL tipping point is plotted on the scatter plot (indicated by the green star). The corresponding 95% confidence intervals for both tipping points are plotted (horizontal and vertical dashed lines). The red squares represent the normal subjects; the blue stars represent the glaucomatous subjects. A lowess smoothing fit (bold black line) to the RNFL-MDB data and its bootstrapped 95% confidence bounds were included to delineate the RNFL-MDB correlation for comparing the consistency of the tipping points. The confidence bounds falling within the 95% confidence regions (central dotted rectangle) defined by the tipping point indicates good one-to-one correspondence of the tipping points.

floor effect may lead to underestimation of the amount of axonal degeneration in the RNFL in relation to VF damage. In our case, the existence and the degree of the floor effect in MDB thickness is not as well studied. As most patients had moderate to advanced glaucoma in this study, investigating the floor effect in the MDB neuroretinal rim thickness and its impact on the determination of the tipping points is warranted for future study. It is interesting to study whether the RNFL and the 3D neuroretinal rim data are interchangeable or complementary in terms of the diagnostic and predictive power of the VF. A recent previous study showed that neuroretinal rim thinning of BMO-MRW may precede RNFL thinning through a nonlinear piecewise regression analysis, echoing the findings in several previous clinical and experimental glaucoma model studies.[47–49] Hence, optic nerve parameters may be earlier indicators of glaucomatous damage compared with RNFL thickness.

The limitations of our study include its cross-sectional nature. Our findings may not apply to individual patients during a longitudinal observation. In addition, clinicians should be cautious when applying our findings to individual subjects, because of the large variation in normal MDB thickness values and possibly varying degrees of optic nerve susceptibility. Patients may start with a thinner or thicker MDB, and their individual tipping point for MDB thickness may vary from the average value we reported. Moreover, using the average structural thickness of the healthy cohort for normalizing the tipping-point location and representing the tissue loss percentage has limitations as well. In particular, besides the individual baseline variability, we are also uncertain about where each subject of the nonsymptomatic healthy cohort is at along the plateau where the neuroretinal structure thickness has virtually no relationship with the VF. Thus, it is important to understand the implications of the wide variation in normal MDB thickness values when applying our tipping-point values for an individual patient. Finally, there are 2 major methodological limitations in this study. First, the normal and glaucomatous populations in the current data set have a significant age difference of 13.7 years (Table 1). Wollstein and colleagues attempted to circumvent this age-mismatch conundrum through adjusting the RNFL values to mean age-adjusted normative values.[27] The age-related effect of MDB and RNFL thickness decrease was not accounted for in this study. It is approximated that the MDB and RNFL thickness reduction is on the order of 1 and 0.4 μm/year.[50,51] As a secondary analysis using values attained from our recent publication,[50] which calculated the age-related thinning (μm/year) of normal MDB thickness for each quadrant and sector (derived from 256 eyes), and setting the mean age of 54.2 years as the reference (Table 1), we adjusted the MDB values to account for the age-related change of the neuroretinal rim thicknesses. The broken-stick analysis was performed, as shown in Table S2 in Supplementary Information (Supplemental Digital Content 1, http://links.lww.com/IJG/A453). The newly obtained tipping-point values are close to the tipping-point values reported in the paper within 25 μm, which is well within the CI widths of each tipping-point value. Hence, with the assumption that there is no age-related coupling to the glaucoma severity as reflected by the VF TD, the impact of the age difference between the healthy and glaucomatous cohorts on the tipping points does not seem to be significant. Future work includes expanding the data set's sample size and including more older healthy subjects to match the ages of the glaucomatous cohort. Second, the demographics of the glaucomatous cohort consist of relatively few early glaucoma or glaucoma suspect subjects and more subjects with advanced glaucoma approaching the structural measurement floor. As discussed above, we speculate that by including more advanced patients, the fitted tipping points may be lower. Future work that expands the sample size of the glaucomatous group to include more glaucoma suspects and early glaucoma subjects would help to refine the location of the tipping points. Of note, recent studies suggested new methodologies in reconciling the discordance in the structure-function relationship for early glaucoma subjects.[52,53] Our analysis and interpretation are in the context where the VF damage was assessed in the decibel scale, for better-assessing patients with moderate to severe glaucoma.

In conclusion, our study analyzed the structure-function relationship between the MDB thickness, a 3D neuroretinal rim parameter easily demarcated in OCT volumetric scans, and VF and identified a clinically relevant tipping point, below which the structural parameter becomes associated with detectable VF deficits. We showed that the MDB thickness could serve as a reliable parameter in identifying the tipping point in regions where RNFL fails to do so. Finally, we also illustrated the correlation between the MDB and RNFL thicknesses and demonstrated the self-consistency of the respective individually identified tipping points. This study may help to guide the physician to know, in general, at which MDB thickness value one should be more concerned about imminent vision loss. Furthermore, artificial intelligence tools like convolutional neural networks and other deep-learning approaches have been applied to study the onset and progression of glaucoma, both structurally and functionally.[54–56] Our results suggest that substantial information about the disease onset is available before the development of functional deficits. As deep-learning approaches are specialized in exploiting such "hidden" information to classify and predict outcomes, our findings also encourage further deep-learning applications to predict the onset of future functional vision loss from retinal structure.

REFERENCES

1. Turalba AV, Grosskreutz C. A review of current technology used in evaluating visual function in glaucoma. *Semin Ophthalmol*. 2010;25:309–316.
2. Alasil T, Wang K, Yu F, et al. Correlation of retinal nerve fiber layer thickness and visual fields in glaucoma: a broken stick model. *Am J Ophthalmol*. 2014;157:953–959.
3. Quigley HA, Addicks EM, Green WR. Optic nerve damage in human glaucoma. III. Quantitative correlation of nerve fiber loss and visual field defect in glaucoma, ischemic neuropathy, papilledema, and toxic neuropathy. *Arch Ophthalmol*. 1982; 100:135–146.
4. Friedman DS, Wolfs RC, O'Colmain BJ, et al. Prevalence of open-angle glaucoma among adults in the United States. *Arch Ophthalmol*. 2004;122:532–538.
5. Quigley HA, Vitale S. Models of open-angle glaucoma prevalence and incidence in the United States. *Invest Ophthalmol Vis Sci*. 1997;38:83–91.
6. Tham YC, Li X, Wong TY, et al. Global prevalence of glaucoma and projections of glaucoma burden through 2040: a systematic review and meta-analysis. *Ophthalmology*. 2014;121: 2081–2090.
7. Kini MM, Leibowitz HM, Colton T, et al. Prevalence of senile cataract, diabetic retinopathy, senile macular degeneration, and open-angle glaucoma in the framingham eye study. *Am J Ophthalmol*. 1978;85:28–34.

8. Quigley HA. Glaucoma. *Lancet*. 2011;377:1367–1377.
9. Wu H, de Boer JF, Chen TC. Diagnostic capability of spectral-domain optical coherence tomography for glaucoma. *Am J Ophthalmol*. 2012;153:815–826 e812.
10. Asrani S, Essaid L, Alder BD, et al. Artifacts in spectral-domain optical coherence tomography measurements in glaucoma. *JAMA Ophthalmol*. 2014;132:396–402.
11. Kim NR, Lim H, Kim JH, et al. Factors associated with false positives in retinal nerve fiber layer color codes from spectral-domain optical coherence tomography. *Ophthalmology*. 2011; 118:1774–1781.
12. Mitchell P, Hourihan F, Sandbach J, et al. The relationship between glaucoma and myopia: the Blue Mountains Eye Study. *Ophthalmology*. 1999;106:2010–2015.
13. Moreno-Montanes J, Anton A, Olmo N, et al. Misalignments in the retinal nerve fiber layer evaluation using cirrus high-definition optical coherence tomography. *J Glaucoma*. 2011;20: 559–565.
14. Fan KC, Tsikata E, Khoueir Z, et al. Enhanced diagnostic capability for glaucoma of 3-dimensional versus 2-dimensional neuroretinal rim parameters using spectral domain optical coherence tomography. *J Glaucoma*. 2017;26:450–458.
15. Khoueir Z, Jassim F, Poon LY, et al. Diagnostic capability of peripapillary three-dimensional retinal nerve fiber layer volume for glaucoma using optical coherence tomography volume scans. *Am J Ophthalmol*. 2017;182:180–193.
16. Liu Y, Jassim F, Braaf B, et al. Diagnostic capability of 3D peripapillary retinal volume for glaucoma using optical coherence tomography customized software. *J Glaucoma*. 2019; 28:708–717.
17. Shieh E, Lee R, Que C, et al. Diagnostic performance of a novel three-dimensional neuroretinal rim parameter for glaucoma using high-density volume scans. *Am J Ophthalmol*. 2016;169: 168–178.
18. Simavli H, Poon LY, Que CJ, et al. Diagnostic capability of peripapillary retinal volume measurements in glaucoma. *J Glaucoma*. 2017;26:592–601.
19. Simavli H, Que CJ, Akduman M, et al. Diagnostic capability of peripapillary retinal thickness in glaucoma using 3D volume scans. *Am J Ophthalmol*. 2015;159:545–556 e542.
20. Tsikata E, Lee R, Shieh E, et al. Comprehensive three-dimensional analysis of the neuroretinal rim in glaucoma using high-density spectral-domain optical coherence tomography volume scans. *Invest Ophthalmol Vis Sci*. 2016;57:5498–5508.
21. Verticchio Vercellin AC, Jassim F, Poon LY, et al. Diagnostic capability of three-dimensional macular parameters for glaucoma using optical coherence tomography volume scans. *Invest Ophthalmol Vis Sci*. 2018;59:4998–5010.
22. Pollet-Villard F, Chiquet C, Romanet JP, et al. Structure-function relationships with spectral-domain optical coherence tomography retinal nerve fiber layer and optic nerve head measurements. *Invest Ophthalmol Vis Sci*. 2014;55:2953–2962.
23. Chen TC, Hoguet A, Junk AK, et al. Spectral-domain OCT: helping the clinician diagnose glaucoma: a report by the American Academy of Ophthalmology. *Ophthalmology*. 2018; 125:1817–1827.
24. Chauhan BC, O'Leary N, AlMobarak FA, et al. Enhanced detection of open-angle glaucoma with an anatomically accurate optical coherence tomography-derived neuroretinal rim parameter. *Ophthalmology*. 2013;120:535–543.
25. Yohannan J, Boland MV. The evolving role of the relationship between optic nerve structure and function in glaucoma. *Ophthalmology*. 2017;124(suppl):S66–S70.
26. Hood DC, Kardon RH. A framework for comparing structural and functional measures of glaucomatous damage. *Prog Retin Eye Res*. 2007;26:688–710.
27. Wollstein G, Kagemann L, Bilonick RA, et al. Retinal nerve fibre layer and visual function loss in glaucoma: the tipping point. *Br J Ophthalmol*. 2012;96:47–52.
28. Park KH, Lee JW, Kim JM, et al. Bruch's membrane opening-minimum rim width and visual field loss in glaucoma: a broken stick analysis. *Int J Ophthalmol*. 2018;11:828–834.
29. Hwang YH, Yoo C, Kim YY. Myopic optic disc tilt and the characteristics of peripapillary retinal nerve fiber layer thickness measured by spectral-domain optical coherence tomography. *J Glaucoma*. 2012;21:260–265.
30. Shoji T, Sato H, Ishida M, et al. Assessment of glaucomatous changes in subjects with high myopia using spectral domain optical coherence tomography. *Invest Ophthalmol Vis Sci*. 2011; 52:1098–1102.
31. Garway-Heath DF, Poinoosawmy D, Fitzke FW, et al. Mapping the visual field to the optic disc in normal tension glaucoma eyes. *Ophthalmology*. 2000;107:1809–1815.
32. Hammer DX, Ferguson RD, Magill JC, et al. Compact scanning laser ophthalmoscope with high-speed retinal tracker. *Appl Opt*. 2003;42:4621–4632.
33. Hammer DX, Ferguson RD, Magill JC, et al. Active retinal tracker for clinical optical coherence tomography systems. *J Biomed Opt*. 2005;10:024038.
34. Ajtony C, Balla Z, Somoskeoy S, et al. Relationship between visual field sensitivity and retinal nerve fiber layer thickness as measured by optical coherence tomography. *Invest Ophthalmol Vis Sci*. 2007;48:258–263.
35. Badlani V, Shahidi M, Shakoor A, et al. Nerve fiber layer thickness in glaucoma patients with asymmetric Hemifield visual field loss. *J Glaucoma*. 2006;15:275–280.
36. Leung CK, Chong KK, Chan WM, et al. Comparative study of retinal nerve fiber layer measurement by stratusOCT and GDx VCC, II: structure/function regression analysis in glaucoma. *Invest Ophthalmol Vis Sci*. 2005;46:3702–3711.
37. Schlottmann PG, De Cilla S, Greenfield DS, et al. Relationship between visual field sensitivity and retinal nerve fiber layer thickness as measured by scanning laser polarimetry. *Invest Ophthalmol Vis Sci*. 2004;45:1823–1829.
38. Harwerth RS, Wheat JL, Fredette MJ, et al. Linking structure and function in glaucoma. *Prog Retin Eye Res*. 2010;29: 249–271.
39. Medeiros FA, Lisboa R, Zangwill LM, et al. Evaluation of progressive neuroretinal rim loss as a surrogate end point for development of visual field loss in glaucoma. *Ophthalmology*. 2014;121:100–109.
40. Quigley HA, Enger C, Katz J, et al. Risk factors for the development of glaucomatous visual field loss in ocular hypertension. *Arch Ophthalmol*. 1994;112:644–649.
41. Liu WW, Margeta MA. Imaging retinal ganglion cell death and dysfunction in glaucoma. *Int Ophthalmol Clin*. 2019;59:41–54.
42. Murphy MC, Conner IP, Teng CY, et al. Retinal structures and visual cortex activity are impaired prior to clinical vision loss in glaucoma. *Sci Rep*. 2016;6:31464.
43. Minckler DS, McLean IW, Tso MO. Distribution of axonal and glial elements in the rhesus optic nerve head studied by electron microscopy. *Am J Ophthalmol*. 1976;82:179–187.
44. Kim SH, Jeoung JW, Park KH, et al. Correlation between retinal nerve fiber layer thickness and visual field sensitivity: diffuse atrophy imaging study. *Ophthalmic Surg Lasers Imaging*. 2012;43(suppl):S75–S82.
45. Rao HL, Zangwill LM, Weinreb RN, et al. Structure-function relationship in glaucoma using spectral-domain optical coherence tomography. *Arch Ophthalmol*. 2011;129:864–871.
46. Hood DC, Anderson SC, Wall M, et al. Structure versus function in glaucoma: an application of a linear model. *Invest Ophthalmol Vis Sci*. 2007;48:3662–3668.
47. Park K, Kim J, Lee J. The relationship between Bruch's membrane opening-minimum rim width and retinal nerve fiber layer thickness and a new index using a neural network. *Transl Vis Sci Technol*. 2018;7:14.
48. Fortune B, Hardin C, Reynaud J, et al. Comparing optic nerve head rim width, rim area, and peripapillary retinal nerve fiber layer thickness to axon count in experimental glaucoma. *Invest Ophthalmol Vis Sci*. 2016;57:OCT404–OCT412.
49. Patel NB, Sullivan-Mee M, Harwerth RS. The relationship between retinal nerve fiber layer thickness and optic nerve head neuroretinal rim tissue in glaucoma. *Invest Ophthalmol Vis Sci*. 2014;55:6802–6816.

50. Antar H, Tsikata E, Ratanawongphaibul K, et al. Analysis of neuroretinal rim by age, race, and sex using high-density 3-dimensional spectral-domain optical coherence tomography. *J Glaucoma*. 2019;28:979–988.
51. Vianna JR, Danthurebandara VM, Sharpe GP, et al. Importance of normal aging in estimating the rate of glaucomatous neuroretinal rim and retinal nerve fiber layer loss. *Ophthalmology*. 2015;122:2392–2398.
52. Mock DC. Letter to the Editor: Challenges to the common clinical paradigm for diagnosis of glaucomatous damage with OCT and visual fields. *Invest Ophthalmol Vis Sci*. 2018;59:5522–5523.
53. Tan O, Greenfield DS, Francis BA, et al. Estimating visual field mean deviation using optical coherence tomographic nerve fiber layer measurements in glaucoma patients. *Sci Rep*. 2019;9:18528.
54. Thompson AC, Jammal AA, Berchuck SI, et al. Assessment of a segmentation-free deep learning algorithm for diagnosing glaucoma from optical coherence tomography scans. *JAMA Ophthalmol*. 2020;138:333–339.
55. Wang M, Shen LQ, Pasquale LR, et al. An artificial intelligence approach to detect visual field progression in glaucoma based on spatial pattern analysis. *Invest Ophthalmol Vis Sci*. 2019;60:365–375.
56. Wang M, Tichelaar J, Pasquale LR, et al. Characterization of central visual field loss in end-stage glaucoma by unsupervised artificial intelligence. *JAMA Ophthalmol*. 2020;138:190–198.

